Water Level Modeling around German Bight

Master Thesis Submitted to

Prof. Dr. Ostap Okhrin

Prof. Dr. Brenda Lopez Cabrera

Ladislaus von Bortkiewicz Chair of Statistics

C.A.S.E.- Centre for Applied Statistics and Economics

Humboldt-Universität zu Berlin

by

Xiaofeng Cao

(522116)

in partial fulfillment of the requirements

for the degree of

Master (M.Sc) in Statistics

Berlin, February 15th, 2012

Acknowledgment

I would first like to extend my sincerest thanks to my supervisor, Prof. Dr. Ostap Okhrin, for his guidance, knowledge and patience throughout this work. I appreciate also my advisor, Prof. Dr. Brenda Lopez Cabrera, for her encouragement and comments.

I would like to express my gratitude to Prof. Dr. Martin Odening in the Department of Agricultural Economics for his support and also to the colleges there, especially to Zhiwei Shen and Stefan Kersting, who enabled me to develop my work. I also appreciate Veronika Blessin for her encouragement in all the time.

Deep gratitude is extended to my best friends, Zografia Anastasiadou and Roberto Villanueva Aguirre, for being with me all the time. Their support and encouragement have been of great value for me. A special thanks is also expressed to Roman Brückner for his guidance on programming so that I could finish this work with the best possible results.

Finally, special recognition is expressed to my dear parents, Xueqin and Zhikui, and also my brother, Yongfeng, for their unconditional love, support and encouragement. No matter what kind of decision I made, they have always been standing by me.

Xiaofeng Cao

Abstract

This work investigates the water level data measured in 18 stations around the German Bight from 1953 to 2006. It is the most useful hydrometric data to measure a water body and to do a forecasting for specific extreme risks. Our water level data are both temporal and spatial. We apply first stochastic time series models to the data on temporal level. The model has four patterns: trend, seasonality, autoregressive components and the heteroscedastic residuals captured by a dynamics conditional volatility model. Two different procedures are applied in this work to model the conditional mean dynamics. After the comparison of the empirical results from all procedures, we get the residuals from the "best" approach. Afterwards we adopt the spatial analysis to the residuals on each day, in order to interpolate for the unobserved locations. Different variogram and Kriging models are applied and compared.

Keywords: water level analysis, seasonality, variogram, Kriging

Zusammenfassung

Diese Arbeit untersucht Schwankungen des Meeresspiegels in der deutschen Bucht anhand der Daten von 18 Messstationen zwischen 1953 und 2006. Mit diesen Daten lassen sich allgemeine Pegelstände bestimmen und das Risiko kritischer Werte vorhersagen. Die Daten werden sowohl zeitlich als auch räumlich analysiert. Auf zeitlicher Ebene wird zunächst ein stochastisches Zeitreihenmodell angewandt, das vier verschiedene Faktoren berücksichtigt: Trend, Saisonabhängigkeit, autoregressive Komponenten und heteroskedastische Residuen, die durch ein bedingtes dynamisches Volatilitätsmodell erfasst werden. Die Dynamik des bedingten Erwartungswerts wird auf zwei verschiedene Arten modelliert. Mit dem optimalen Ansatz können die Residuen für jeden Tag der Beobachtungsperiode bestimmt werden. Die räumliche Analyse der zeitbedingten Residuen ermöglicht es, Pegelstände auch für unbeobachtete Orte zu berechnen. Verschiedene Variogramm und Kriging Modelle werden dafür benutzt und verglichen.

Schlagwörter: Analyse des Pegelstands, Saisonabhängigkeit, Variogramm, Kriging

Contents

1. Introduction

The Quality Status Report 2000 for the North-East Atlantic (referred as QSR (2000) later) stated that over the last 100 years the mean annual sea level in German Bight had increased by 30 cm. Besides, extreme waves, caused by storm surges, are potentially dangerous to the human's activities. Along the German coast, waves interact with spring tides lead to often extreme high water level, for example the North Sea flood of 1953 and 1962. As an example the North Sea flood of 1962 took away of hundreds lives in Hamburg and made massive damage in the whole western Germany. Examples such as these motivate to study the forecasting of water levels.

A "water level" is the level of the surface water body. They record the water depth above a normal zero level and are one of the most useful pieces of hydrometric data.

There are often confusion between the term "water level", "water table" and "sea level". Water tables measure groundwater, but water levels are a measure of surface water. Both fluctuate under changes in climatic and hydrographical conditions. Sea level (or mean sea level) measures the average height of the ocean's surface, which is more like a "still water level", so we can use it as a standard to determine land elevation.

In this work we study water level data around the German Bight. German Bight is one part of the relatively shallow southern North Sea and in this area Elbe and Weser discharge huge volumes of water into the sea at their river mouths. Tidal and wave activities can be also strong in both rivers, see QSR (2000).

Our data are both temporal and spatial, therefore the analysis takes into account both spatial and temporal correlations. Although over the last decade some spatial-temporal models have been created, such as space-time Kriging or dynamics models for non-stationary spatio-temporal data (Stroud et al. (2001)), our analysis is relatively traditional, using time series analysis and spatial statistics separately.

Plenty of papers have been published introducing and applying univariate time series models to weather data. Campbell and Diebold (2002), Campbell and Diebold (2005) for instance have applied a time series approach to daily average temperature in U.S. cities and used the trend, seasonality and cyclical patterns to reveal conditional mean dynamics. They also modeled on conditional variance dynamics. Benth and Saltyte Benth (2005) used a mean-reverting Ornstein-Uhlenbeck process to model daily average temperature variation, then fitted the volatility dynamics with a Fourier Series and AR process. Härdle et al. (2011) created a local adaptive model to estimate the seasonality and volatility with an optimal smoothing parameter, instead of a Fourier Series.

In this work we model the water level data on the same components as in Campbell's model for conditional mean dynamics, but with two main different procedures. After comparison of the empirical results, the "best" model will be chosen as the final model for our analysis.

Since water level varies over time, it is possible to group the data into specific periods and perform spatial analysis in each period. Kumar and Ahmed (2006) have carried out such research

for ground water level. They calculated monthly variograms and used their average to create two common variograms for the entire year. Their study shows that it is not always necessary to calculate variograms separately for all periods. But to be more accurate, we apply spatial analysis to the residuals achieved from the time series model on each day. Therefore we can interpolate the daily value for unobserved locations, using the variograms and Kriging models. The Ordinary Kriging and Universal Kriging are applied to the data, then we compare the empirical results and choose one proper model. Furthermore we do Kriging in subareas to see if we can achieve more precise predictors.

The thesis is structured as follows. In section 2 the data are presented. In section 3 both time series models are outlined, and each is followed by analysis of its empirical results. We then choose the "best" approach and perform further analysis before the spatial analysis in section 4. We introduce the variogram and Kriging models in section 5 and present the application results in section 6. Finally, we present our conclusion.

2. Data

2.1. About the Data

In this section our historical water level data are presented and cleaned for analysis. Our dataset contains daily water level observations measured in cm from 01 January 1953 to 31 December 2006, measured in the 18 stations (Details in Figure 2.1).

We obtained the dataset from Aon Benfield, a division of Aon Corporation which functions as a reinsurance intermediary and full-service capital advisor.

Water level is influenced strongly by tides which are caused by the gravitational forces of the moon and sun acting on the oceans; the water level is therefore measeured twice per day also around the German Bight, due to semidiurnal (twice daily) tides in the North sea. There were five days with three observations each: 17.01.1984, 20.11.1987, 08.10.1988, 26.02.2002, 21.12.2003 (reason unknown). No missing values appear in the dataset. Amid concerns over risks, such as overflow, the maximum value on each day is chosen as our daily water level data for the temporal and spatial analysis. To simplify the calculation, all leap days are removed. In total, we have 19,710 observations in each of the 18 stations with the time length of 54 years.

On top of this we took the coordinates of all 18 stations in the dataset from Pegel Online, and converted them from the Gauss-Krueger System used locally in Germany to the World Geodetic System - a standard consisting of longitude and latitude which can be used directly in `R` program for spatial analysis.

From the map we can see that the stations are either near-shore or in the rivers inland, therefore we choose the stations Cuxhaven and Bremen-Brueckner (later referred to as Bremen) as the representatives of each kind of locations respectively.

2.2. Historical Water Level

Before modeling the water level data, we require some overall information about the daily water level.

First, we calculate the maximum and mean of each month in Bremen and Cuxhaven separately for the whole 54 years (see Figure 2.1).

We can observe that there are statistically significant trends in all monthly data by running linear regressions. Especially, the monthly maximum water level in Bremen has a clearly increasing trend which can be detected in Figure 2.2. Table 2.1 shows us the coefficients of the linear regressors. Based on Table 2.1 we can also conclude that there was an upward tendency in the water level in the German Bight. For instance, from 1953 to 2006, the maximum of water level in Bremen increased around 70 cm, but only 23 cm in Cuxhaven . It is clear that in the past half

Figure 2.1.: The 18 measure stations in the German Bight. The source of the orignal map: Pegel Online, editted by me.

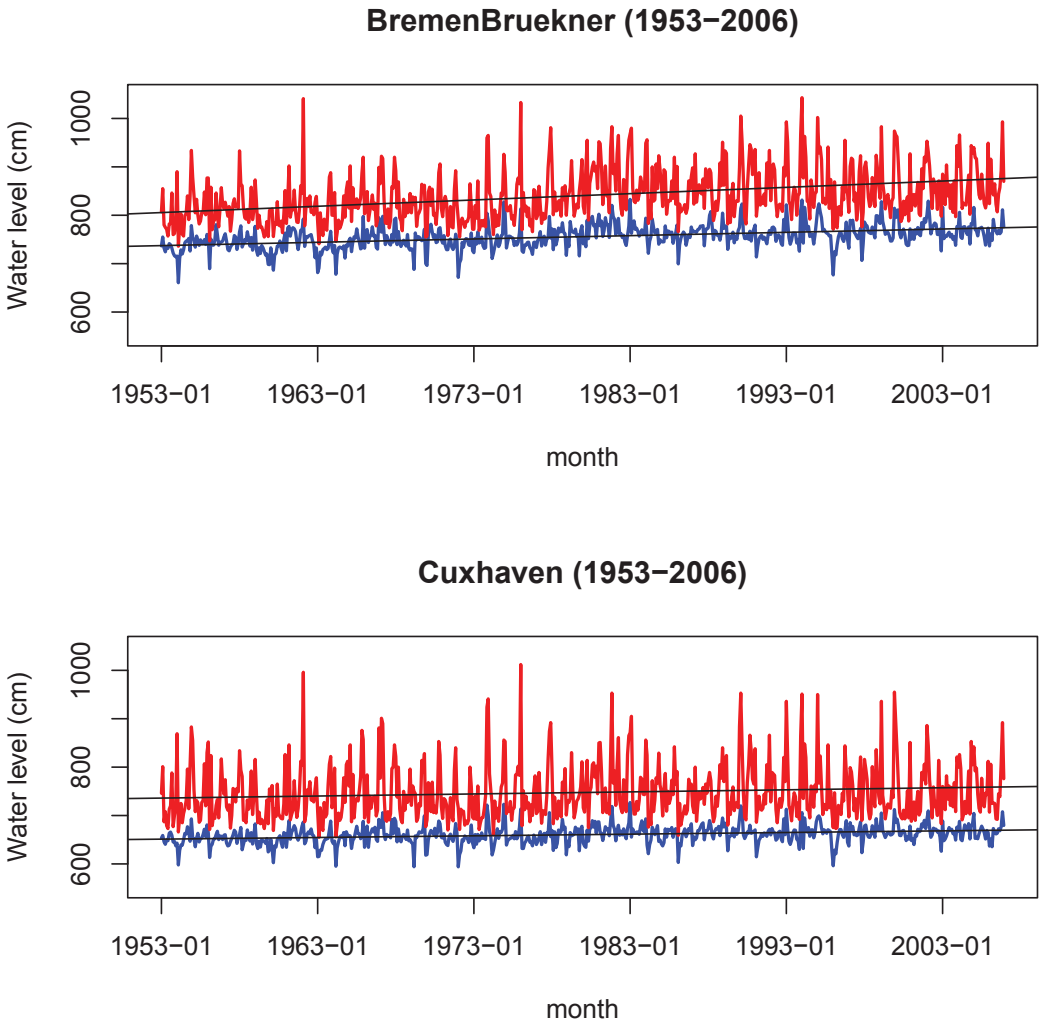

Figure 2.2.: The Monthly data plots in Bremen and Cuxhaven.

Parameter	Bremen Maximum	Bremen Mean	Cuxhaven Maximum	Cuxhaven Mean
intercept	805.43672	737.2	735.9690	651.2
slope	0.10857	0.05716	0.03561	0.02855

Table 2.1.: The coefficients of parameters of the linear regressions for the monthly data in period 1953-2006.

Station	Min.	1st Qu.	Median	Mean	3rd Qu.	Max.
Bremen	504.0	730.0	754.0	755.8	778.0	1043.0
Schulau	406.0	660.0	684.0	687.2	710.0	1125.0
Cuxhaven	440.0	637.0	658.0	660.5	680.0	1012.0
Hoernum	405.0	579.0	598.0	602.0	619.0	905.0

Table 2.2.: The summary statistics of the daily water level in four stations.

century the maximal water level has increased with time in this area, leading to an increase in the risk of an extreme water situation such as overflow.

Figure 2.3 plots the daily water level series for the last 5 years (2002-2006) of the sample in Bremen and Cuxhaven. This time series plot reveals a regular and repeated seasonal pattern: a sharp peak occurs each January, after which the water level increases slightly and slowly during the summer, although the curves are not so apparent. Figure 2.4 shows this fluctuation more clearly. We take the mean over years of daily water level first and then draw box plots for each month in 4 stations: Bremen and Schulau from the inland stations and Cuxhaven and Hoernum from the near-shore stations. We see that most of the stations follow a similar pattern, with the slight exception of Hoernum in the autumn, and therefore we can use a common time series model for all stations. The summary statistics in these four stations can be found in Table 2.2.

QSR (2000) reports how the North Sea climate varied over the past 150 years, and the most extreme decadal changes have occurred from the 1960s to the present day. It is possible that water level has been also strongly influenced by climate change. We therefore analyze our data structure over the whole 54 year period, in order to determine if changes have been extreme and if it is reasonable to apply one common model for seasonality or volatility over a relatively long period of time. We group all 54 years into three equal subintervals, each 18 years in length, then take the mean over years of daily water level data from the corresponding interval and plot them with their respective confidence intervals. In order to be more clear, we plot only the curves of the first and last subintervals in Figure 2.5. The solid blue line in the upper panel denotes the mean over years of daily water level in the subperiod from 1989 to 2006, and the dotted blue lines are the corresponding confidence intervals. The red lines reveal the same in the subperiod from 1953 to 1970.

We can see that the mean over years of daily water level in Cuxhaven can be covered well by the confidence interval of the other subinterval, but in Bremen both confidence intervals do not overlay much in winter. However it still indicates that the water level data have similar structures in all subperiods. We can also draw the conclusion that the mean over years of daily water level in the last subinterval is clearly larger than those in the first subinterval. It proves from another perspective that the water level increased over time in the past years.

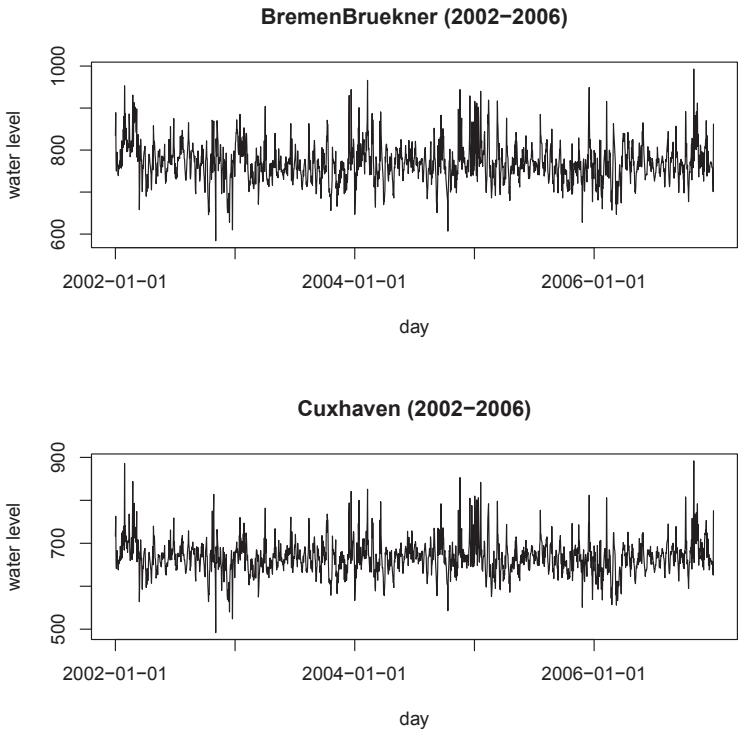

Figure 2.3.: The last 5 years data plots in Bremen and Cuxhaven.

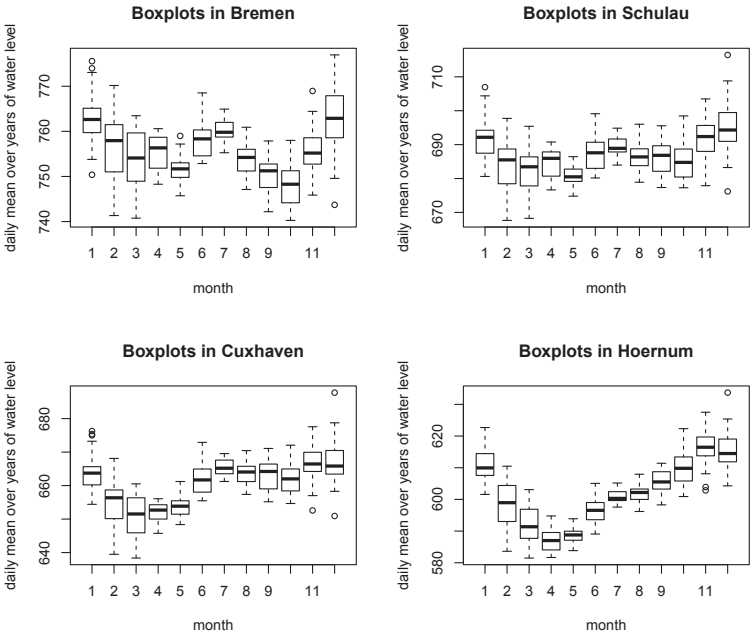

Figure 2.4.: The boxplots of the mean over years of water level in 4 stations:Bremen, Schulau,Cuxhaven and Hoernum.

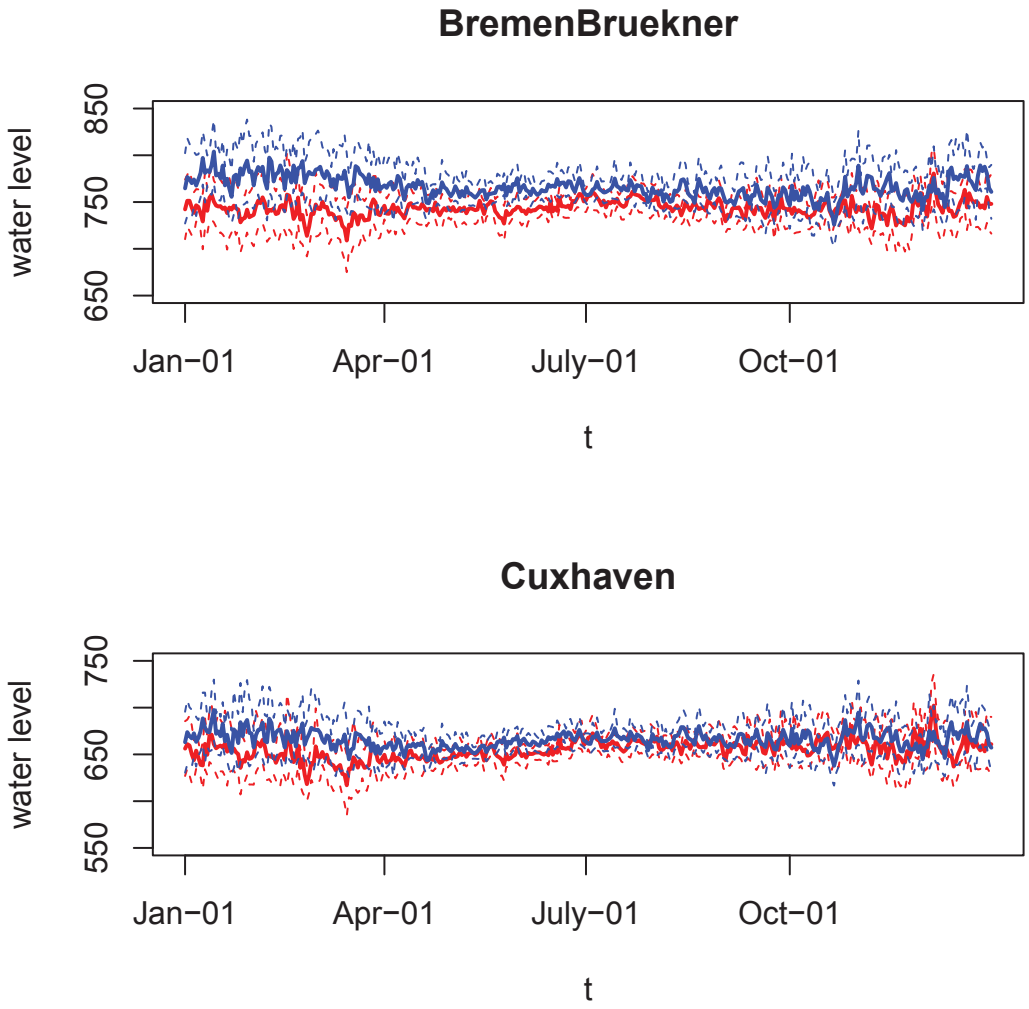

Figure 2.5.: The mean over years in subintervals and their corresponding confidence intervals.

3. Univariate Time Series Modeling

From the plots in the section 2, we know that our data displays trend and seasonal patterns. As mentioned in Campbell and Diebold (2005), a low ordered Fourier series can help us to midel this seasonality, allowing us to perform numerically stable estimations for large amounts of data. Another factor which also affects the dynamics is the so-called cyclic component -both Benth and Saltyte Benth (2005) and Campbell and Diebold (2005) use an Autoregressive process to capture it in their models. Furthermore, temperature volatility is demonstrated by a seasonal GARCH model in Campbell and Diebold (2005), but Benth and Saltyte Benth (2005) explain the variance of the temperature only by a distinctive seasonal pattern.

To model our daily water level data, we can decompose the time series into the following components: trend, seasonality, AR process and residual. We can estimate the components step by step as in the Benth model or regress water level on the four components all together in the same way as Campbell and Diebold (2005). Therefore we construct two models using three different approaches.

We use the same conditional mean functions of Campbell and Diebold for the conditional mean dynamics of our water level (details in Model A). We estimate the seasonal component indirectly together with other parameters. Therefore the deseasonalized water level today is regressed on the original water level in previous days. This procedure is time-consuming and not easy to compute, and it might also cause uncertainty to parameter estimates, see Benth and Saltyte Benth (2011). Afterwards we model the conditional volatility dynamics using only a Fourier series, because our empirical results show that there is no significant AR part in the residuals of water level.

Model B is a stepwise procedure. Since we estimate each component step by step, the seasonal mean is obtained directly from the water level observations and then, after removing the seasonal mean, we model the AR process. That is, we regress the deseasonalized water level directly on itself. There are two different possible steps to deseasonalize water level: (1) detrending first and then eliminating the seasonality; (2) detrending and deseasonalizing jointly. We will perform both to choose a better way. Such procedures are not only much simpler to compute compared to Model A, they also more reasonable to explain the facts of water level. Finally use the same conditional volatility model as in Model A.

3.1. Model A: Campbell and Dieblod Procedure

3.1.1. Theoretical Framework

$$Y_t = Trend_t + \Lambda_t + \sum_{l=1}^{L} \rho_l Y_{t-l} + \eta_t \tag{3.1}$$

where

$$\begin{aligned} Trend_t &= \beta_0 + \beta_1 t \\ \Lambda_t &= \sum_{p=1}^{P} \left[a_{c,p} \cos\left\{ 2\pi p \frac{d(t)}{365} \right\} + a_{s,p} \sin\left\{ 2\pi p \frac{d(t)}{365} \right\} \right] \\ \eta_t &= \sigma_t \varepsilon_t \\ \sigma_t^2 &= b_0 + \sum_{q=1}^{Q} \left[b_{c,q} \cos\left\{ 2\pi q \frac{d(t)}{365} \right\} + b_{s,q} \sin\left\{ 2\pi q \frac{d(t)}{365} \right\} \right] \\ \varepsilon_t &\sim iid(0,1) \end{aligned} \tag{3.2}$$

In equation (3.1) we use a simple linear model for the trend and account for the seasonality via the Fourier series Λ_t. At the same time we denote $d(t)$ as a repeating step function which circulates in the time interval [1:365].

Using the same approach as in Campbell and Diebold (2005), we estimate the model in two steps. In the first step, applying the ordinary least square method, we regress daily water level on constant, trend, Fourier series and AR process all together, and get the residuals η_t. Next we take the average of squared η_t - $\bar{\eta}_t^2$ - and use equation (3.2) to estimate volatility. In this way we can replicate the estimations of volatilities for all 54 years and take the inverse of the square root of the replications as our weights in equation (3.2). We can then find the estimator of ε_t after running the weighted least square regression.

To choose the orders of the Fourier series and AR process, we use the Akaike and Schwarz information criteria. But as mentioned by Koehler and Murphree (1988), AIC can cause over-estimations of the parameters. BIC is therefore preferred. When both indicate different orders for our model, we use the smallest BIC as the criterion. Since we have data from 18 measuring stations, it is possible that different orders of Fourier series and AR might occur. In these cases we take the maximum orders for both Fourier series and AR processes from each station and use these in our general model.

3.1.2. Results

Based on the Schwarz information criterion, we choose the orders of Fourier series and AR process for each measuring station (see Table 3.1), then set the maximal order from all stations to be $p = 2$, $q = 29$. Here one should note that the order of the AR processes is quite large. This means past water levels have influence on current values for a relatively long time, although the coefficients of most lags are relatively small. In Bremen, for instance, the coefficients of the first and second lags are 0.5681 and 0.1201, but 12 of the 29 values are not statistically significant given the confidence level of 0.05. We can use this relatively large value of the AR order to capture the long term dynamics, similarly to the temperature model of Campbell and Diebold (2005).

After the first step, running the OLS regression, the results of the conditional mean model reveal statistically significant trends in water level in all stations. Although the values of the trends are quite minor, for example $a_1 = 0.0004565$ in Bremen, water levels increased significantly in the long time period. Over 54 years, the water level in Bremen rose by 8.998 cm, and by 5.408 cm in Cuxhaven - these values should not be ignored, and they might indicate an association

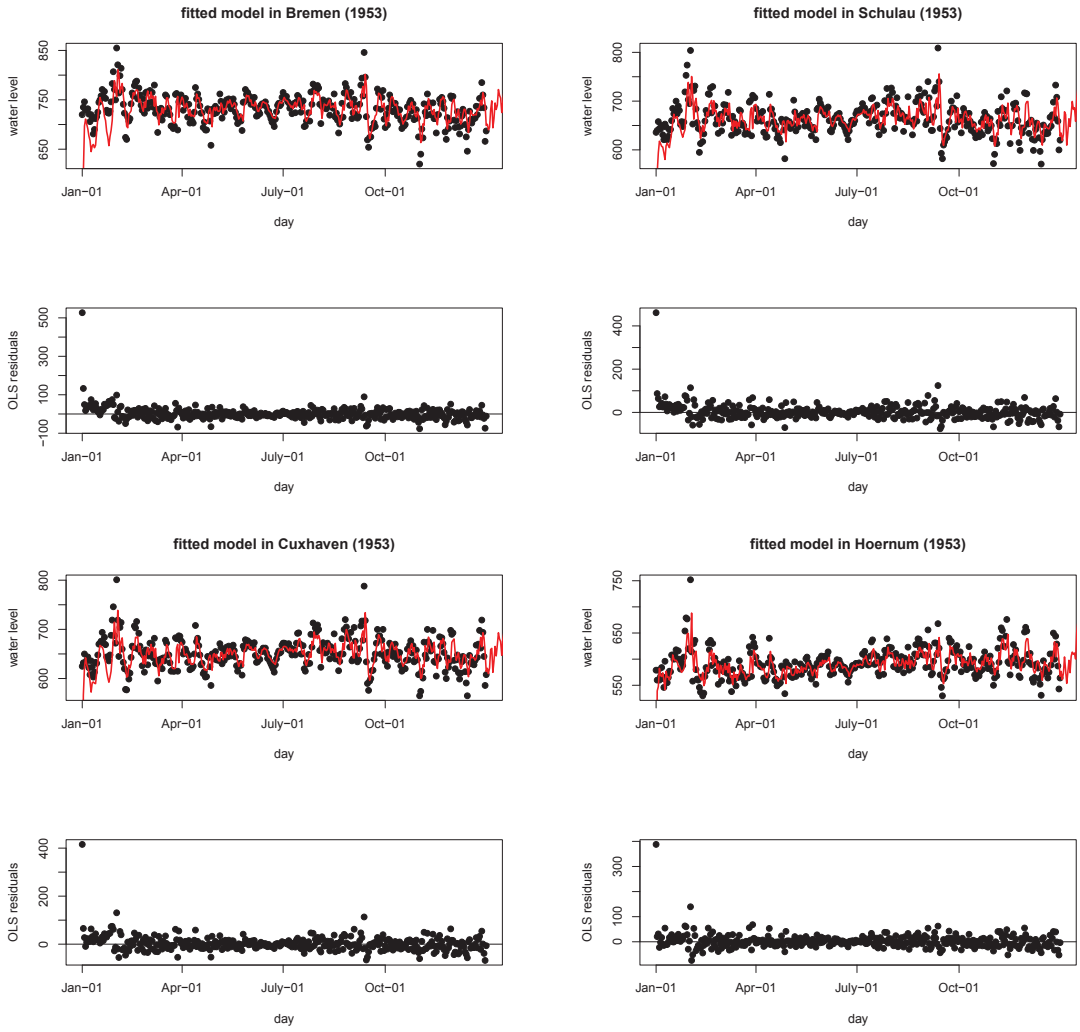

Figure 3.1.: The fitted OLS model of water level in four stations and their residuals from Model A.

with global warming. Based on the dataset of more than 100 years from Helgoland, there is a weak positive trend in the temperature data, and the rate of increase is about $0.6C^{\circ}/yr$, see QSR (2000).

Figure 3.1 shows the fitted line of our OLS model in water levels and their corresponding residuals η_t. Worth mentioning is that the first points in all residual plots are an extreme outlier, perhaps due to the cut-off lags of the AR processes in the model.

Moreover, Figure 3.2 show the fitted line of volatility estimation model, where we use a Fourier series with order 2. It is obvious that the residuals fluctuate widely in the winter months, but in summer they tend to narrow down. One possible reason is that strong winds during winter affect water surface movement.

As is known, there are conditional heteroscedacities influencing the accuracy of the models and therefore the value of residuals, so we run a WLS regression to eliminate this pattern. The plots

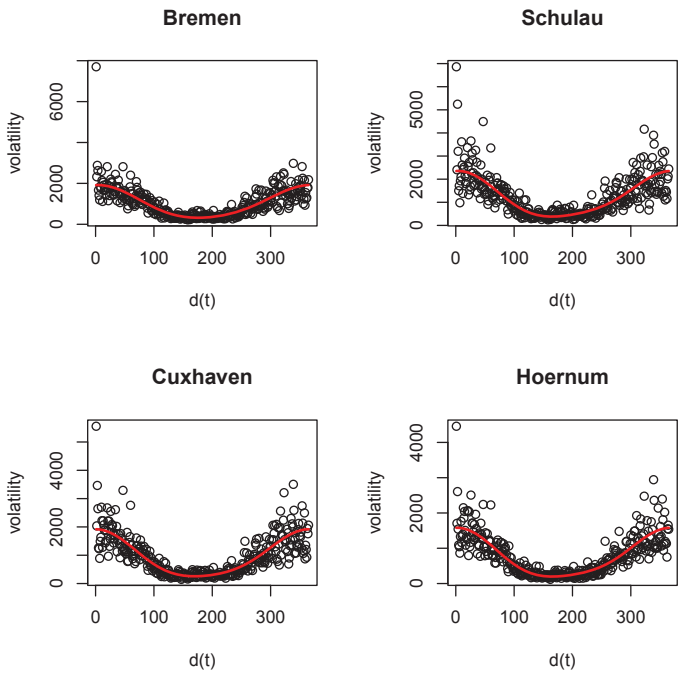

Figure 3.2.: The fitted model of volatilities in four stations from Model A.

of the fitted WLS model and $\hat{\varepsilon}_t$ respectively are found in the appendix.

In Figure 3.3 the QQ-plots show that the residuals do not follow the QQ-line closely, and the tails spread out in most stations. As well as this, the normality tests, both Anderson-Darling (AD) and Kolmogorov-Smirnov (KS), give us very small P-valueS. We should therefore reject the null hypotheses that the residuals of the whole period are not normally distributed.

The R^2 of the conditional mean model after removing the conditional heteroscedacity, are between 0.41 and 0.59, meaning our model explains between 41% and 59% of the variance of the water level.

There is no autocorrelation between different lags of either OLS residuals $\hat{\eta}_t$ or WLS residuals $\hat{\varepsilon}_t$ and we plot the ACF and PACF of $\hat{\varepsilon}_t$ in Figure 3.4. The P-values of the Durbin-Watson (DW) test are smaller than the significant level $\alpha = 0.05$, and again show that first autocorrelation does not exist for all stations. It is the difference between the temperature data in Campbell model which still has obvious cyclic part in the volatility. For our water level data, this model can remove all significant AR parts.

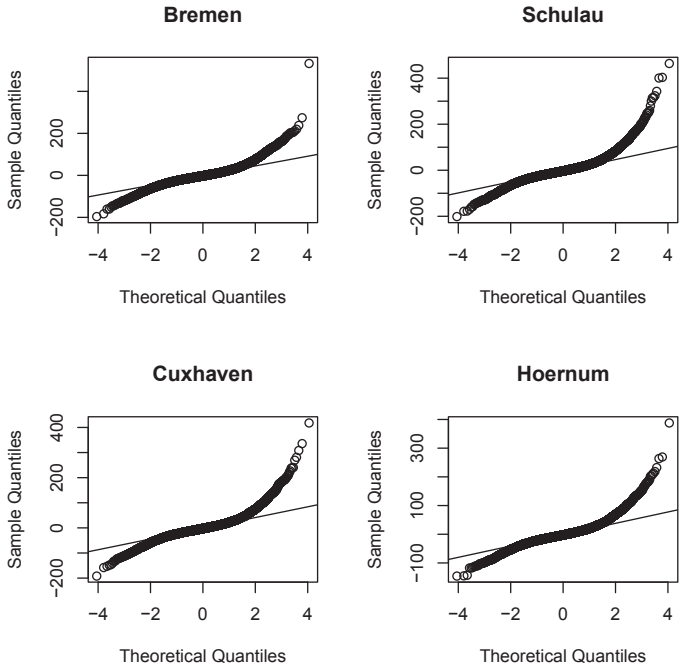

Figure 3.3.: The QQ-plots of $\hat{\varepsilon}_t$ in four stations from Model A.

	ModelA			Model B		
Station	P	L	Q	P	L	Q
Bremen	2	28	1	1	24	1
Brokdorf	2	2	2	5	24	1
Buesum	2	28	2	5	24	1
Cuxhaven	2	28	2	5	24	1
Dagebuell	2	5	2	5	26	1
Emden	2	28	2	5	24	1
Hamburg	1	14	2	5	26	1
Helgoland	2	28	2	5	24	2
Hoernum	2	3	2	2	29	2
Husum	2	28	2	5	24	1
Leerort	2	28	2	5	24	1
List	2	3	2	5	29	1
Oldenburg	1	28	1	5	24	3
Schulau	1	14	2	5	27	1
Stadersand	1	14	2	5	27	1
Wilhelmshaven	2	29	5	1	24	1
Wittduen	2	29	1	2	24	2
Zollenspieker	1	14	1	2	24	1
Maximum order	2	29	2	5	29	3

Table 3.1.: The orders of Fourier Series P, Q, and AR process L in Model A and B for all stations.

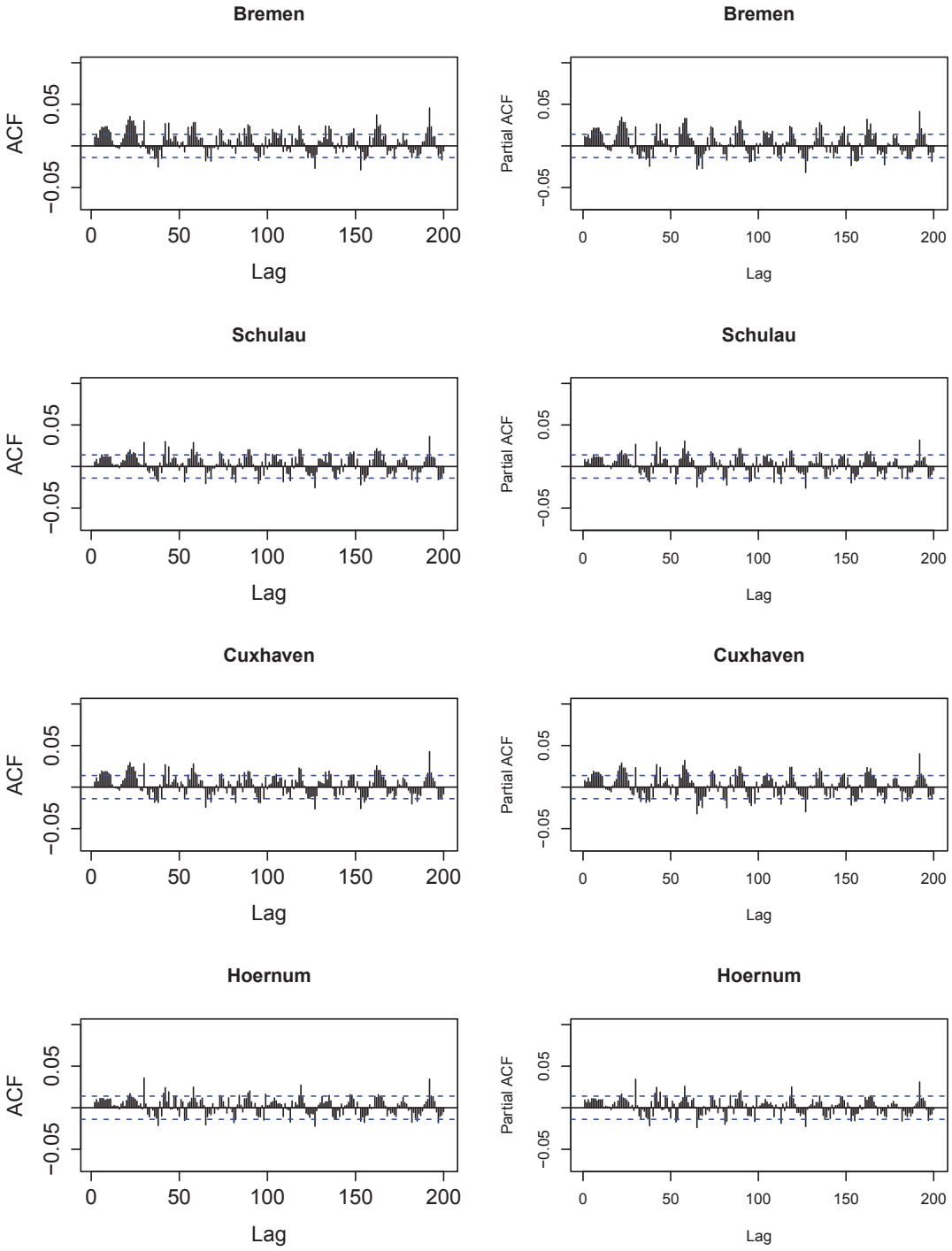

Figure 3.4.: The ACF and PACF plots of ε_t in four stations from Model A.

3.2. Model B: Step by Step Modeling

3.2.1. Theoretical Framework

3.2.1.1 Modeling the seasonality

We consider the following model to estimate all the trend, seasonality, and AR components step by step, similar to the approach which Benth and Saltyte Benth (2005) used for temperature. As mentioned before, we deseasonalize the water level in two possible methods: (1) detrending first and then deseasonalizing; (2) detrending and deseasonalizing jointly.

Method (1)

$$
\begin{aligned}
Y_t &= \beta_0 + \beta_1 t + U_t \\
U_t &= \Lambda_t + X_t \\
X_t &= U_t - \Lambda_t
\end{aligned}
$$

First, we need detect if there is a deterministic long-term trend in the water level. We use the same simple linear regression with intercept to fulfill the aim.

Next we take the mean over years of U_t to estimate the seasonality, so that we can get the same seasonality model for each year. In the next step we repeat this procedure 54 times for all years to obtain the seasonal pattern Λ_t for the whole time period.

$$
\Lambda_t = \sum_{p=1}^{P} \left[a_{c,p} \cos\left\{ 2\pi p \frac{d(t)}{365} \right\} + a_{s,p} \sin\left\{ 2\pi p \frac{d(t)}{365} \right\} \right] \tag{3.3}
$$

where $d(t)$ is the same step function in the interval [1:365] as in Model A. After that we can subtract the data to find the deseasonalized water level.

Method (2)

$$
\begin{aligned}
Y_t &= \Lambda_t + X_t \\
X_t &= Y_t - \Lambda_t
\end{aligned}
$$

Alternatively, we can also take first the mean over years of daily water level, to estimate the trend and seasonality jointly. Afterwards we detrend and deseasonalize the water lever data.

$$
\Lambda_t = \beta_0 + \beta_1 d(t) + \sum_{p=1}^{P} \left[a_{c,p} \cos\left\{ 2\pi p \frac{d(t)}{365} \right\} + a_{s,p} \sin\left\{ 2\pi p \frac{d(t)}{365} \right\} \right] \tag{3.4}
$$

3.2.1.2 Modeling the AR process and volatility

After the first step, the seasonal mean of the water level data get removed. Now we model the cyclical component by an AR process and then analyze the conditional volatility dynamics using also a Fourier series to demonstrate the seasonal pattern, just as in model A.

$$X_t = \sum_{l=1}^{L} \delta_l X_{t-l} + \eta_t$$

And:

$$\begin{aligned} \eta_t &= \sigma_t \varepsilon_t \\ \sigma_t^2 &= b_0 + \sum_{q=1}^{Q} \left[b_{c,q} \cos\left\{ 2\pi q \frac{d(t)}{365} \right\} + b_{s,q} \sin\left\{ 2\pi q \frac{d(t)}{365} \right\} \right] \\ \varepsilon_t &\sim iid(0,1) \end{aligned}$$

During the whole step by step process, we still use AIC and BIC as the criteria to choose the order of Fourier series and the AR process. The choosing process remains identical as in Model A.

3.2.2. Results

In model B, we run the regression in two ways, but it turns out that the second approach gives us the smaller value of RMSE (see Table 4.1). We therefore focus on method (2), and model the AR process and volatility.

After we fit the seasonal component with a Fourier series, we plot in Figure 3.5 the fitted Fourier series curves of daily water level in year 1953, with $q = 5$. The right panels are the plots of corresponding $\hat{X}_t$.

In Figure 3.6 we plot the estimated ACF and PACF of the residuals of the detrended and deseasonalized water level, which shows there are autoregressive components. Therefore we regress X_t on lagged X_{t-l}. Based on the smallest BIC, the order 27 of AR processes is chosen for each station (see table 3.1).

After the analysis of the conditional mean dynamics, we estimate the volatility model and the order 2 is chosen for the Fourier series which denotes the cyclical component (see Table 3.1). The plots of the volatility model (Figure 3.8) reveal this clear sign of seasonal heteroscedasticity, -that is, the variations in winter are much larger than in summer.

After removing heteroscedasticity, we check the ACF and PACF of $\hat{\varepsilon}_t$. In Figure 3.7 there is no longer any significant autocorrelation. The QQ-plots of $\hat{\varepsilon}_t$ (see Figure 3.9) also show that $\hat{\varepsilon}_t$ is not normally distributed, but the ourliers have much smaller values than those from Model A.

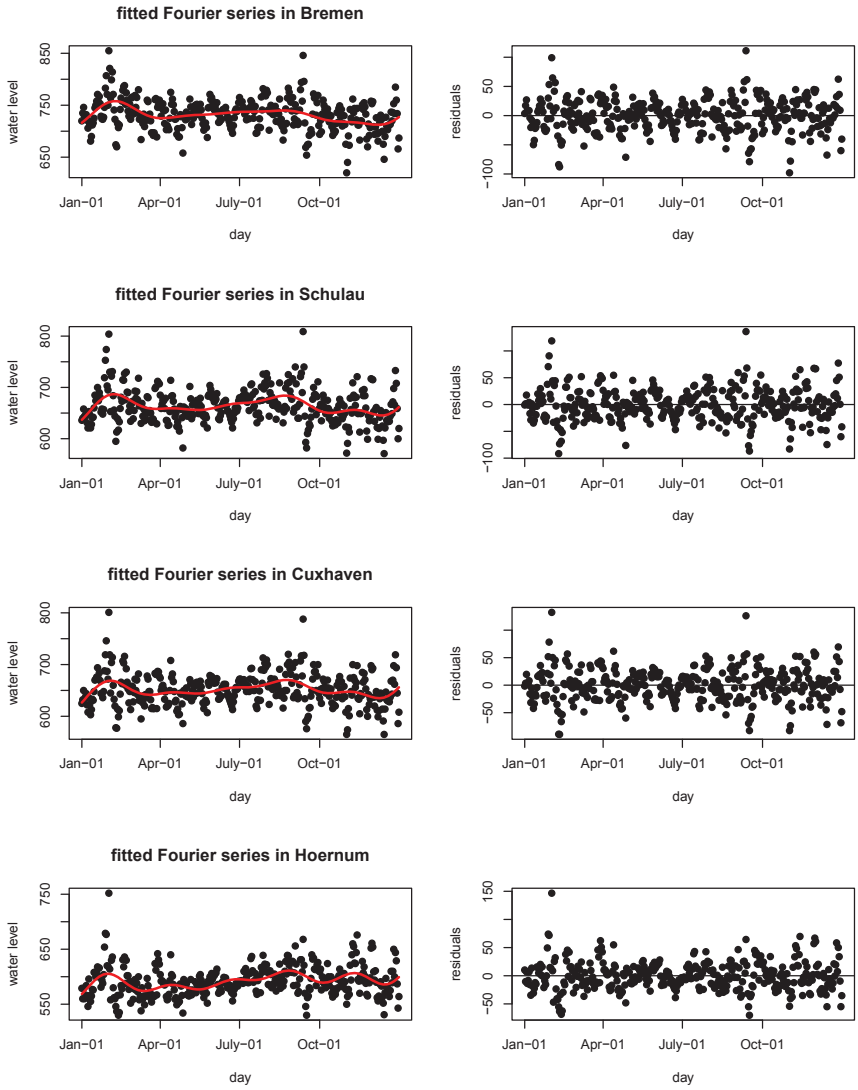

Figure 3.5.: The fitted detrending and Fourier model (1953) in four stations from Model B.

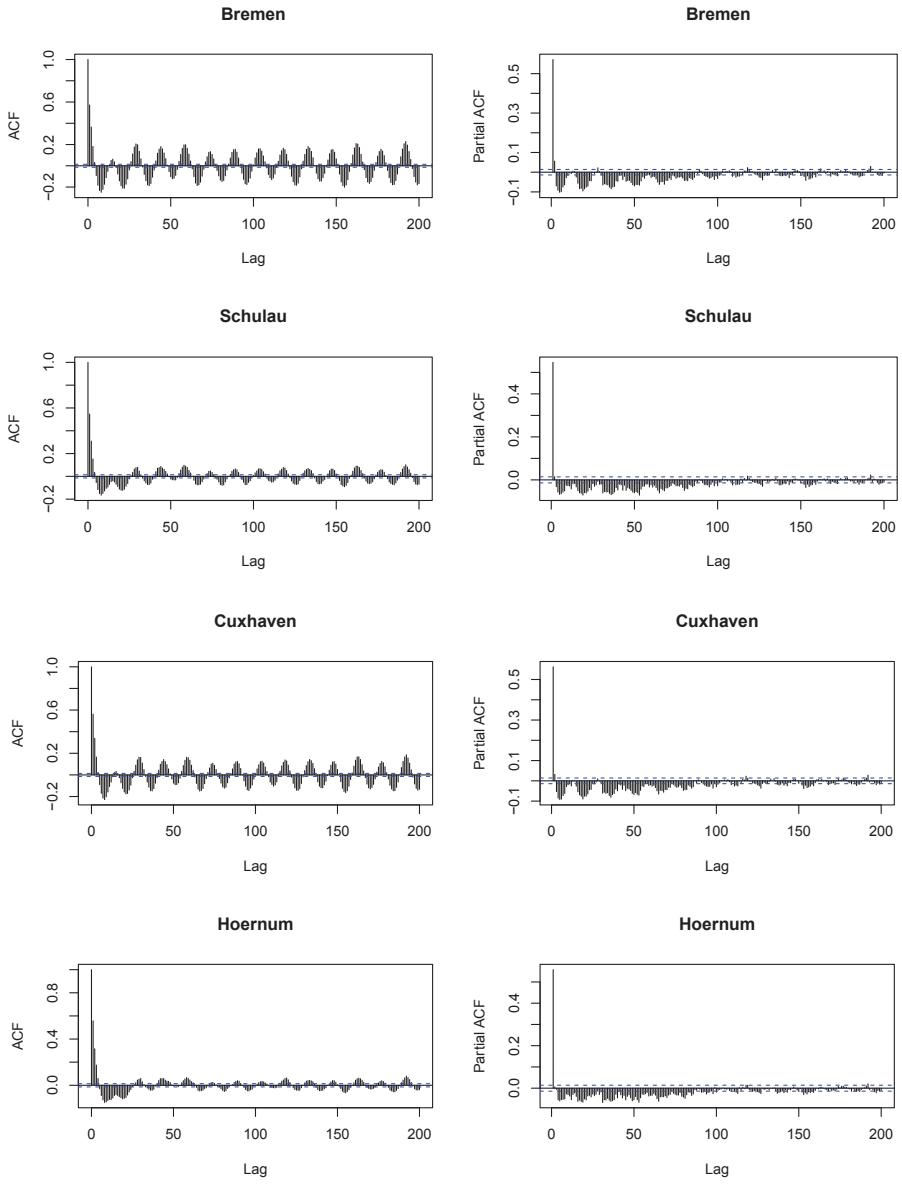

Figure 3.6.: The ACF and PACF plots of residuals after detrending and deseasonalizing in four stations from Model B

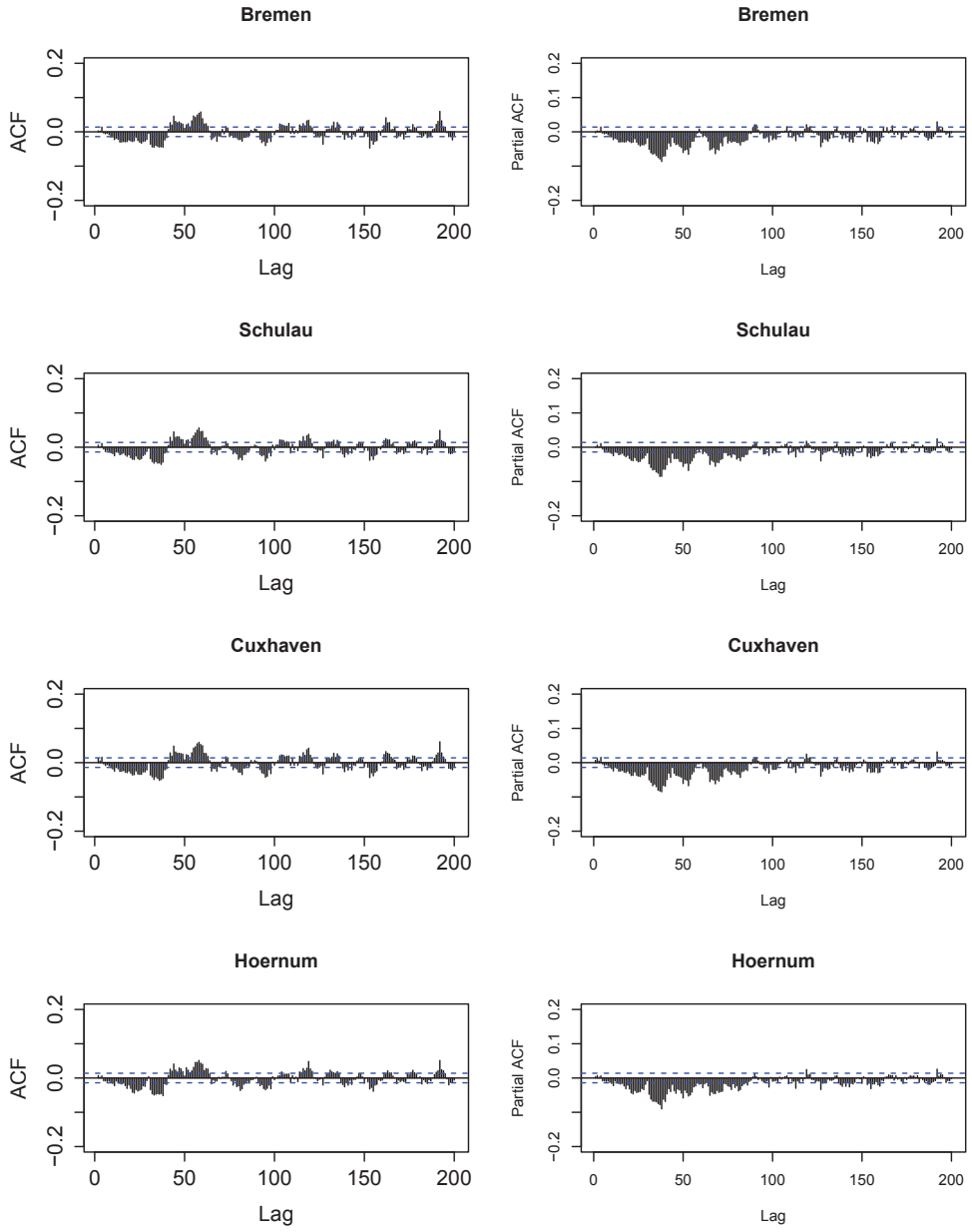

Figure 3.7.: The ACF and PACF plots of residuals $\hat{\varepsilon}_t$ in four stations from Model B.

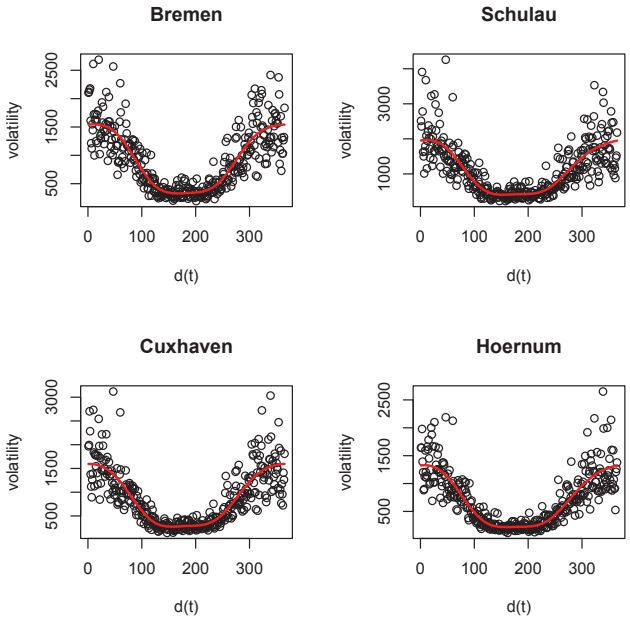

Figure 3.8.: The fitted volatility model in four stations from Model B.

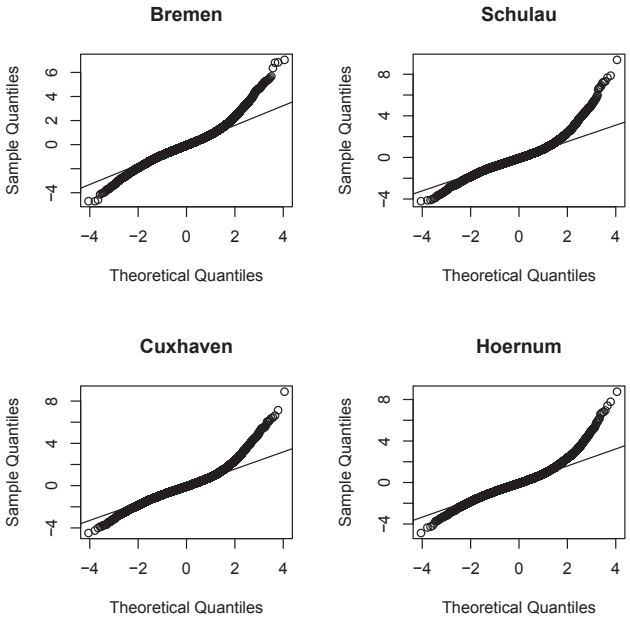

Figure 3.9.: The QQ-plots of $\hat{\varepsilon}_t$ in four stations from Model B.

4. Time Series Model Choosing and Analysis

4.1. Comparison of Time Series Models

Both Model A and Model B give us the residuals without autocorrelation, and the normality hypothesis for the whole time period is rejected. Since it is not possible to compare the adjusted-R^2 of different procedures, we need to compare of the root-mean-square errors (RMSEs) to choose the model which better fits the data.

The RMSEs from all our models are listed in Table 4.1 The simultaneously detrended and deseasonalized version of model B wins out with the smallest RMSE of 124.7292, and we take this model and its residuals for further analysis. All estimators are presented in Tables A.1, A.2 and A.3 in the appendix.

We noticed outliers in both tails of the whole-period QQ-plots, and here we attempt to detect these outliers. The maximum residuals $\hat{\varepsilon}_t$ in most stations (although not in Dagebuell, Hoernum or Oldenburg) appear on the 16_{th} February 1962, the day of the North Sea flood disaster. The flood was caused by an enormous windstorm and affected all the German Bight from the coast to the rivers, leading to totally 315 death in Hamburg and the destruction of 60,000 homes, see Lamb and Frydendahl (1991).

As shown before, the residuals over the whole 54 years periods are not normally distributed, due to too many outliers. But it is worth investigating how the residuals in each year are distributed. For instance, The QQ-plots (Figure 4.1) of residuals in the year 1953 show that the majority follow the QQ-line well, apart from a few outliers on the tails. In this year, the maximum outliers appeared either on 1 February 1953 ($t = 32$) or 12 September 1953 ($t = 255$). The 1953 North Sea flood happened on the night of Saturday 31 January 1953 and morning of 1 February 1953. But the AD-test on the residuals in 1953 produces a small P-value, therefore we reject the hypotheses of normality, although we do not draw the same conclusion based on the QQ-plots.

4.2. Cluster Analysis and Correlations

Before we begin the spatial analysis, some forward work is necessary. Spatial techniques require the data to be relatively highly correlated. Before revealing the correlation structure of the

	Model A	Model B (Method 1)	Model B (Method 2)
RMSE	132.1294	126.1735	124.7292

Table 4.1.: The RMSE of all time series models.

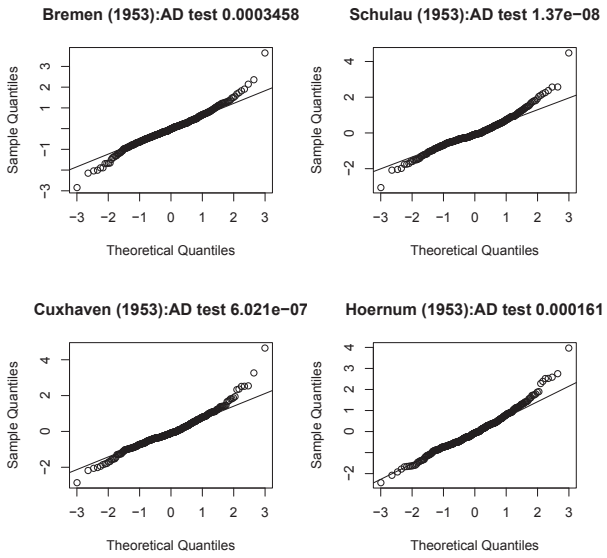

Figure 4.1.: The QQ-plots of residuals $\hat{\varepsilon}_t$ (1953) in four stations from Model B.

residuals $\hat{\varepsilon}_t$ of all stations, we perform the cluster analysis to show how the data of all stations are clustered. Afterwards we arrange the order of the stations and plot the correlation image, based on the cluster relation between all stations (Figure 4.2).

The lower panel of Figure 4.2 is the hierarchical tree plot obtained by using the complete linkage method for hierarchical clustering. The vertical axis denotes the linkage distance based on Euclidean distance, and in the horizontal direction the respective stations are linked together into clusters. It is clear that List, Hoernum, Wittduen, Dagebuell and Husum, located in the north of Helgoland, are linked into one cluster (referred to as Group A later). Brokdorf, Hamburg, Schulau, Stadersand and Zollenspieker, which are located nearby the river Elber, generate another cluster. As can be seen in the correlation image, stations in the same cluster are highly correlated. Oldenburg shows the lowest correlation with others, and especially with Group A. This is mainly because it is located in a river running in a west-east direction and the river does not flow directly to the German Bight. Overall, however, the correlation between each station is higher than 0.7, and we can therefore apply spatial analysis to the residuals.

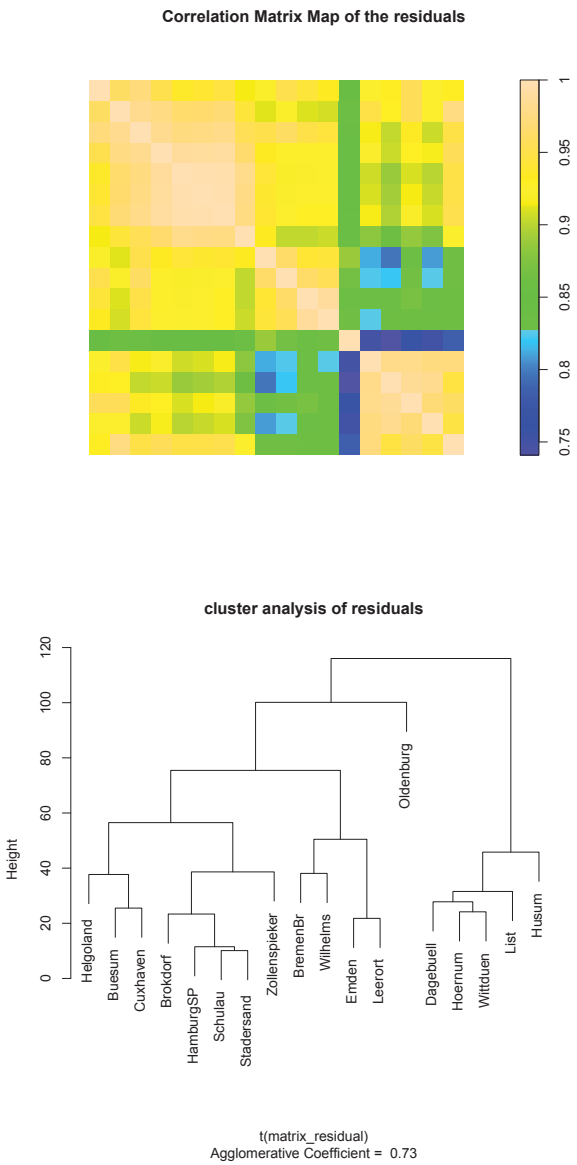

Figure 4.2.: The Correlation image of $\hat{\varepsilon}_t$ of all stations (the upper panel) and the cluster relation (the lower panel).

5. Spatial Models

It is possible that data are correlated when they are located near each other in terms of time or space. It is therefore worth studying our data from a spatial perspective, since our original data are collected at 18 stations with specific coordinates which play an explicit role in the analysis.

In our case, the basic spatial components are the 18 spatial irregular locations $\{S_1,\ldots,S_{18}\}$ and the data $\{Z(S_1),\ldots,Z(S_{18})\}$ which are detrended, deseasonalized and have their autoregressive component eliminated, that is ε_t on each day t in each station. We can use spatial point process to summarize current data and predict unobserved data.

As suggested in Cressie (1993), we can take the following steps when dealing with spatial data: graphing and summarizing, detecting information about the assumptions, estimating spatial relationships (normally through the variogram model), interpolating by Kriging and finally assessing the procedure.

Before applying the spatial model to our data, we first present the theoretical framework.

5.1. Variogram

Kriging is based on the knowledge of the variogram or the covariance. In this paper, we concentrate on the former, because the covariance requires a more crucial assumption for its existence than the variogram and its estimator depends only on a constant, whereas the variogram estimator is also tolerant to a random function, see Olea (1999).

The random data $\{Z(S_i)\}$ at certain points $\{S_i : i = 1,\ldots,n\}$, as defined before, exhibit "instrinsic stationarity" which follows the formular:

$$\mathrm{E}\{Z(S_i+h)-Z(S_i)\}=0$$

Then

$$\mathrm{Var}\{Z(S_i+h)-Z(S_i)\}=2\gamma(h)$$

is known as the variogram, and the semivariogram is equal to $\gamma(h)$ (Cressie (1993)). The classic estimator of the variogram, given by Mathern, is as follows:

$$2\gamma(h)=\frac{1}{|N(h)|}\sum_{N(h)}\{Z(S_i+h)-Z(S_i)\}^2$$

where $Z(S_i)$ is the value at locations S_i and $N(h)$ is the number of experimental pairs sepa-

rated by the distance h between each pair, see Olea (1999). Similarly to time series analysis, sometimes we can also use a so called "spatial lag" to illustrate the distance h.

Unfortunately, there are no statistical tests to evaluate an experimental variogram and check if it approximates the theoretical variogram closely. Normally we can visually compare an experimental variogram with fitted theoretical variogram values by a plot to see how "close" they are. Actually, in geostatistical analysis, visual inspection is required throughout the modeling process. If we want to detect a model automatically, however we can use one of two methods: maximum likelihood estimation and least squares.

Cressie (1993) argues that maximum likelihood methods rely on Gaussian distributional assumptions too strongly and give us biased estimators. On the other hand, there are some limitations in least square methods as well. For instance, when using least squares, one can not calculate parameters directly from the data, so we need to estimate the experimental variogram at a few lags preliminarily, see Olea (1999). Three least squares methods are available: ordinary least squares, weighted least squares and general least squares.

Estimation of experimental variograms presents other problems. For instance, the expression of calculating implies the mean square average of the difference depends only on the distance h, meaning we have to determine either the isotropy or anisotropy of the data. One option for dealing with this anisotropic problem is to use the anisotropic variogram (Details in Cressie (2011)), or to compute the directional variogram after setting the main direction. It has been suggested, however, that this problem can be ignored with very small sample sizes, and one can estimate the data as if it were omni-directional. For example, Haberlandt (2007) compares prediction performance for hourly precipitation data in South-East-Germany and finds there is no significant difference between isotropic and anisotropic variograms, despite the presence of anisotropy in the data.

In practice, there are a number of different variogram models. The most commonly used models, such as Gaussian, Spherical, power, Exponential or Cubic, have their own analytical expressions.

For example, the Gaussian semivariogram model is:

$$\gamma(h) = C\left[1 - e^{-3\frac{h}{a}^2}\right]$$

where C is the sill, and a is the range, see Olea (1999).

The Stein-Matern function, which is one of the Matern class function, developed by Stein (1999), is:

$$\rho(h) = \frac{\pi^{\frac{1}{2}\phi}}{2^{\kappa-1}\Gamma(\kappa+\frac{1}{2})a^{2\kappa}}(a|h|)^{\kappa}K_{\kappa}(a|h|)$$

where K_{κ} is a modified Bessel function, and κ is an additional smooth parameter that is flexible to the local behavior of the random field on which the spatial interpolates strongly depends. The larger is κ, the smoother the variogram. As $\kappa \to \infty$, we obtain the Gaussian model as an extreme case.

5.2. Kriging

In the 1950s a South African engineer, D.G. Krige, found an empirical method during his work to estimate ore content. In 1963 Mathern developed this method to predict optimally in spatial linear regression and named it after Krige, see Cressie (1990). Kriging was referred as an estimator untill 1991, when Cressie called it a predictor, see Cressie (1993).

Kriging is a stochastic technique for spatial prediction which takes the form of a generalized linear regression and uses the minimum mean square error as the absis for an optimal predictor, under the assumption of the second-order properties of the spatial process. Importantly, there is no distributional assumption for Kriging. Put simply, we can use a linear combination of weights at known points to estimate the value at any unknown point in that area, see Cressie (1993).

Today many different forms of Kriging have been developed and applied, including Simple Kriging, Ordinary Kriging, Universal Kriging, Block Kriging and Cokriging. Of these, Simple Kriging takes the most basic, but at the same time it also has limited applicability requiring some assumptions to find weights. We therefore se Ordinary Kriging and Universal Kriging with our data.

5.2.1. Ordinary Kriging

According to Cressie (1993), Ordinary Kriging is defined under the following assumptions.

Model assumption:

$$Z(S_i) = \mu + e(S_i),$$

Where $\mu \in \mathrm{R}$ is unknown, $e(\cdot)$ is a white-noise process with mean zero and variance $\sigma_e^2 \geq 0$, and n is the number of locations. $e(\cdot)$determines the variogram $2\gamma(\cdot)$. The predictor assumption is:

$$\hat{Z}(S_0) = \sum_{i=1}^{n} \omega_i Z(S_i) \quad with \quad \sum_{i=1}^{n} \omega_i = 1$$

Where $\hat{Z}(S_0)$ is the predictor at new location S_0, $Z(S_i)$ are the random variables at location S_i, and ω_i are weights assigned to each location S_i.

The Ordinary Kriging predictor is similar to a Simple Kriging estimator, but with constraints so that the weights sum to one and μ is known. Because the weights sum up to one, a uniformly unbiased μ is guaranteed. We can then get an optimal predictor with minimum mean squared prediction error, see Cressie (1993).

As we mentioned before, we perform Kriging based on the variogram model. Once S_0 is set, we need to minimize:

$$\sigma_e^2 = \mathrm{E}\left\{Z(S_i) - \hat{Z}(S_0)\right\}^2,$$

where σ_e^2 is the mean square prediction error, often called the Kriging variance or Kriging standard error, which is associated to the measure of uncertainty (Cressie and Wikle (2011). We need therefore to minimize:

$$\mathrm{E}\left\{\sum_{i=1}^{n}\omega_i Z(S_i) - Z(S_0)\right\}^2 - 2\lambda(\sum_{i=1}^{n}\omega_i - 1)$$

Where λ is the Lagrange multiplier to ensure $\sum_{i=1}^{n}\omega_i = 1$. We will skip the mathematical details for solving the minimization, only to reveal how S_0 is used in the Ordinary Kriging model.

5.2.2. Universal Kriging

If we relax the assumption of constant μ in Equation 5.6 and assume instead an unknown linear combination of known functions $q_k(\cdot)$, the Ordinary Kriging predictor changes to a Universal Kriging one.

The Universal Kriging predictor is

$$\hat{Z}(S_0) = \sum_{k=0}^{K}\hat{\beta}_k q_k(S_0) + \sum_{i=1}^{n}\omega_i(S_0)e(S_i) \quad with \quad q_0(S_0) = 1 \tag{5.1}$$

where $\hat{\beta}_k$ is the coefficient of the $k-th$ external predictor $q_k(S_0)$ at location S_0, K is the number of predictors, $e(S_i)$ are the residuals interpolated by Ordinary Kriging, see both Cressie (1993) and Olea (1999).

The first part of the right side of (5.1) is sometimes called the drift, and the most common form of $q_k(S_0)$ is a simple linear combination of the geographical coordinates. The second part presents the zero-mean regression residuals, see Hengl et al. (2004).

As argued in Hengl (2011), Universal Kriging is mathematically equivalent to Regression Kriging and Kriging with external drift, since all give the same prediction. In many papers, Universal Kriging is thus reserved solely for the case in which we are predicting only with coordinates. If we want to include additional variables, such as altitude or other geological information, we can use to a Regression Kriging predictor. Since we are only using coordinates in this paper, the Universal Kriging approach is more appropriate. This also implies a combination of regressions with Kriging.

Both Ordinary Kriging and Universal Kriging share the properties of unbiased predictor and minimum mean square errors. As well as this, they can be interpolated exactly and are automatically corrected for clustering, see Olea (1999). Universal Kriging, however, is more robust for inadequate assumptions or misspecifications of parameters. It also requires only an estimator of the variogram of the residuals, rather than the variogram of the original variable required by Ordinary Kriging.

5.3. Assessment

We can use a cross validation test to determine the best variogram model for our analysis. To evaluate the predictors of different spatial models, Hengl (2011) suggests following five criteria for application:

1. the overall mapping accuracy through RMSE at valid points;
2. the biasness, mean absolute error (MAE);
3. if the model is robust or sensitive;
4. if the model is reliable;
5. if the process is much time-consuming.

6. Application of Spatial Model

After performing univariate time series analysis of the water level data in all measure stations, we identify the residuals ε_t with geographical locations but without any border information.

Before presenting the results of the spatial model, we can get an overall feeling for our data by looking at the spatial characteristics of ε_1.

`geoR` is a good tool for analysis of spatial data in R, which was developed at Lancaster University, UK. With this package, the data and their locations can be visualized as in Figure 6.1. The upper-left panel is the map with longitude on the x-axis and latitude on the y-axis. The colors and symbols indicate the different concentrations of data at each location: for example, the uppermost triangle denotes the location of Helgoland and its value. The upper-right and lower-left panels show the relation between the data values and their coordinates. No clear trend appears in both horizontal and vertical directions. The lower-right panel provides the histogram of the density of $\hat{\varepsilon_1}$.

Plots of $\hat{\varepsilon_i}$ with $t = 1,\ldots,4$ (Figure 6.2) show how the spatial data differ on each day. We therefore need to specify the spatial model on each day. The summary statistics on these days are in Table 8.5 in the appendix.

Table 6.1 gives us the distance in kilometers and the correlations of the residuals between Helgoland and other stations.

We are concerned with the overflow caused by waves, especially under the risk of storms. Waves travel along the water's surface effortlessly and keep changing with the wind. The speed of surface waves are affected by factors such as wind, the density of water, the pull of gravity, and their wave lengths. Speed therefore varies with time. The fastest observed speed of surface waves was around 900 km/hr, observed in 1960, and was caused by tsunamis. The peak speed of the North Sea flood of 1962 reached almost 200 km/hr. Most normal waves, however, are not that fast waves. For instance, waves with a period of 10 seconds has a speed of 56 km/hr, see Anthoni (2000), meaning it takes 1- 3 hours to travel from Helgoland to other stations.

To explore the spatial structure of the data, the empirical variogram is obtained by ordinary least squares, since the variogram model can not only provide the base for the further calculation of Kriging, but also help us to detect if the data are anisotropic.

Figure 6.3 shows the directional variogram in four directions, revealing that our data are anisotropic. In R program 0° is the north direction, and degrees subsequently increase in the clockwise direction. At 90° and 135°, which are the west-east direction and the north-west to south-east direction respectively, we have spatial dependence in most spatial lags, but fairly few in other directions.

Our data is anisotropic, meaning the dependence between any two locations is tied not only to the magnitude but also the direction of the distance. Normally an underlying physical process may cause this problem. To detect the cause of the anisotropy of our data, we need know which

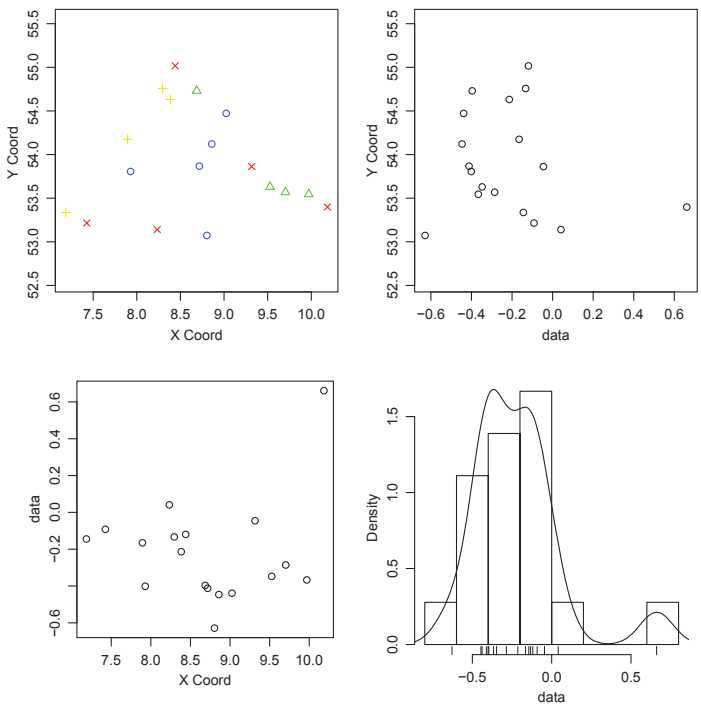

Figure 6.1.: The spatial description map when $t = 1$.

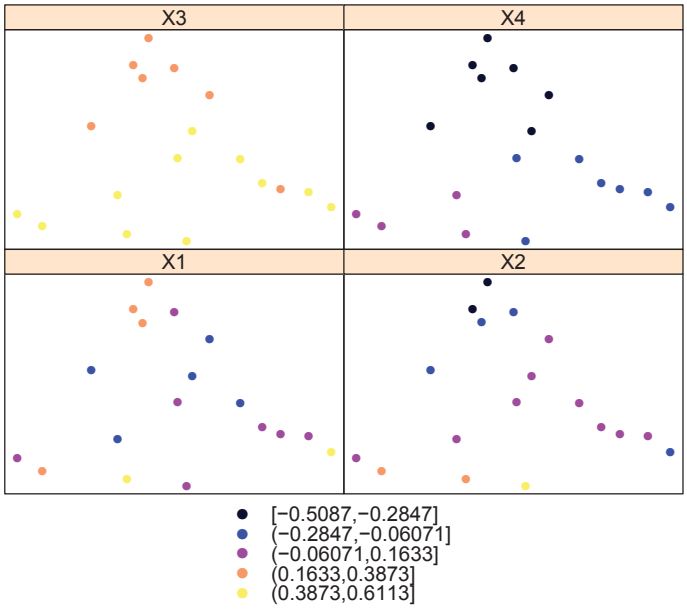

Figure 6.2.: The spatial map when $t = 1, \ldots, 4$.

Station	Distance	Pearson correlation	Spearman correlation
Helgoland	0.00000	1.0000000	1.0000000
Bremen	136.44756	0.9213391	0.9182694
Brokdorf	99.18372	0.9526263	0.9549765
Buesum	63.12795	0.9618449	0.9617349
Cuxhaven	63.72566	0.9730995	0.9744883
Dagebuell	80.28177	0.9251747	0.9268744
Emden	104.20642	0.9436860	0.9445832
HamburgSP	153.08655	0.9365706	0.9333536
Hoernum	69.86399	0.9310145	0.9269637
Husum.	80.44090	0.9306193	0.9331177
Leerort	111.09978	0.9324364	0.9324060
List	100.00066	0.9268341	0.9191170
Oldenburg	117.24969	0.8465363	0.8706368
Schulau	136.46210	0.9403010	0.9371352
Stadersand	122.96853	0.9457874	0.9440135
Wilhelms	75.26438	0.9520375	0.9500555
Wittduen	59.88494	0.9569123	0.9559898
Zollenspieker	173.54043	0.9131235	0.9023764

Table 6.1.: The distance in km and the correlations between the Helgoland and other stations.

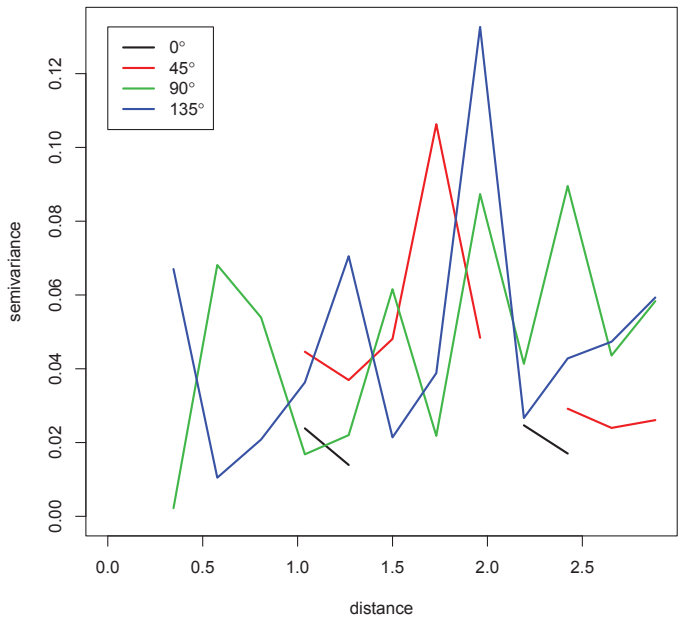

Figure 6.3.: The directional variogram in four directions when $t = 1$.

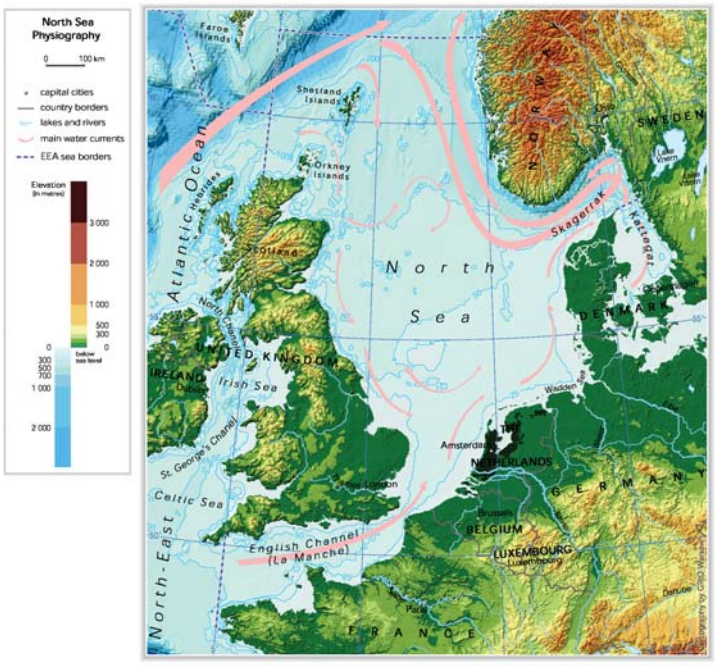

Figure 6.4.: The map of the ocean current in North Sea. Source: European Environment Agency.

factors might affect the water level first. Apart from the hydrographical factors, such as tides, waves, and ocean currents, there are also other climatic and geographical factors which have an effect on water level, for instance winds, storms, the bottom topography, and salinity.

In order to better understand these factors, an image of the ocean current in the North Sea is presented (Figure 6.4). We can see the main currents form a cyclic circulation over the North Sear and flow from south to north in the German Bight. However, since the winds blow in that area in various directions over time, it is possible they are not the main reason for the data anisotropy. In our case, some of the stations are on the shore, and the others are in the river inland. The differentiation of water and land in geology between any two stations appears to be the main reason. Since the sea water flows from the sea to land, and the two rivers Elbe and Weser run into the sea, they fit the 90° and 135° directions and might be the main reasons for the anisotropy in our data.

Before Kriging analysis, we need to create a regular grid map of interpolated points as the overall prediction region, and then find the minimum and maximum values of the longitude and latitude coordinates.

Next we overlay the observed locations on the prediction grid. It should be noted here that we can make the grid more or less intensive, depending on the threshold we give in Table 6.2, (see Figure A.1 in Appendix).

We use package `automap` to achieve automated interpolation, by fitting the variogram and producing the predictors. Here we plot the Ordinary Kriging estimators and the corresponding variogram for $t = 1, 2$, so we see that the fitted spatial model changes on different days, see

	Longitude	Latitude
Maximum	10.18538	55.01658
Minimun	7.18629	53.07312
Grid threshold	12.00000	10.00000

Table 6.2.: The setting of the grid map. The grid threshold here denotes the number of the gridcells in each direction.

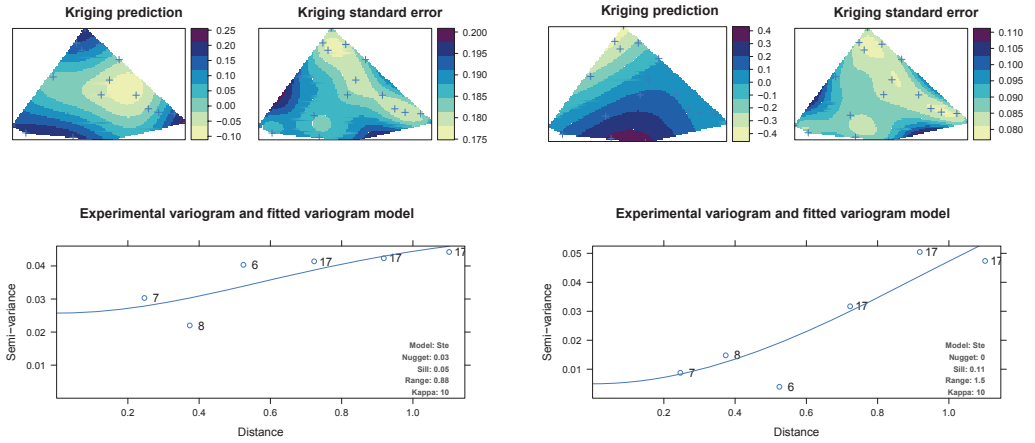

Figure 6.5.: The fitted variogram and Ordinary Kriging model when $t = 1$ (left) and $t = 2$ (right).

Figure 6.5.

The lower panel of Figure 6.5 is the plot of the variogram model, where the points denote the values of the experimental variogram and the number beside presents the number of experimental pairs in that spatial lag. The smooth blue line is the automated fitted theoretical variogram model. We can also see directly from the plot the corresponding values of nugget, sill and range of the theoretical variogram model. In this case, for both $t = 1, 2$ the Stein-Matern model is chosen but with different values of nugget, sill and range.

The upper two plots are the visualization of the prediction map and the prediction error map on a grid with around 5000 gridcells, allowing for a relatively "continuous" prediction map.

The left plot gives us all predictors obtained by Ordinary Kriging in color. The darker the blue, the higher value of the predictor we get. When $t = 1$, the prediction values are in the interval of $[-0.1, 0.25]$, but they differ in various locations. The blue crosses are the measure locations.

The right map is the relative prediction error map with the label on the right side. It tells us how good we expect the predictors to be, based on the variogram and the data locations. The brighter the color is, the smaller the standard prediction error or the less uncertain is the prediction. We should mention, if we change the thresholds, thereby changing the grid of prediction, the visualization of prediction error will show that the uncertainty also changes.

Figure 6.6 shows the visual Universal Kriging predictor map on the grid plot with 120 gridcells, where the plots are in square form and appear discontinuously. When $t = 1$, the Stein-Matern Model is also chosen as theoretical variogram, but with nugget equal to 0.02 and range equal

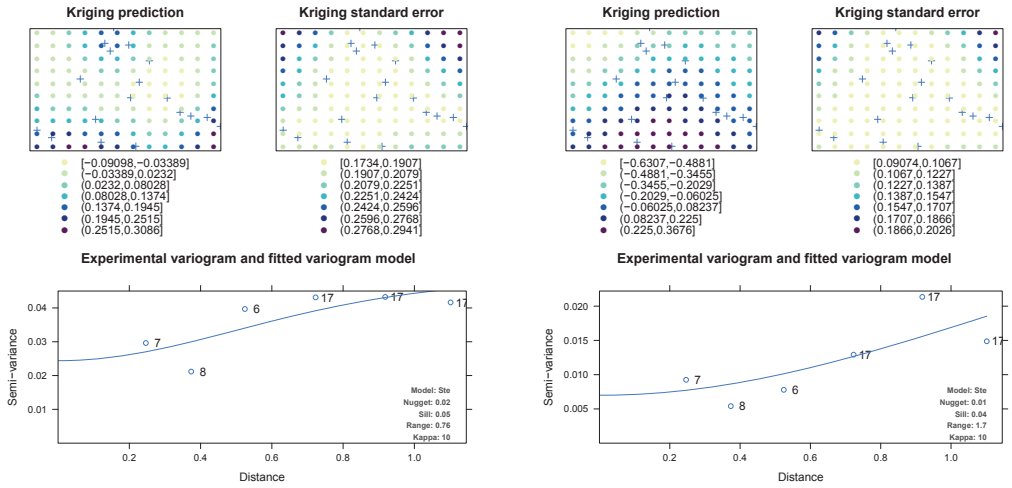

Figure 6.6.: The fitted variogram and Universal Kriging model when $t = 1$ (left) and $t = 2$ (right).

t	SSE Ordinary Kriging	SSE Universal Kriging
1	0.00584	0.00662
2	0.00741	0.00185
3	0.00044	0.00001
4	0.00673	0.00035

Table 6.3.: The sum of squares error between the sample variogram and the fitted variogram model for both Kriging models.

to 0.76 which are smaller than the respective values from Ordinary Kriging. Given the same prediction grid, we compare the sum of squares error between the sample variogram and the fitted variogram model for both the Ordinary and Universal Kriging models.

Comparing the visualizations of the Ordinary Kriging and Universal Kriging, it becomes clear that, for $t = 1, 2$, the theoretical variogram fits well for both models. Both Ordinary Kriging and Universal Kriging maps show gradual change in different locations, and it is difficult to judge by eye which model gives us smaller prediction error. But the Universal Kriging predictor and also the prediction errors have a relatively larger interval than those of the Ordinary Kriging model.

Table 6.3 gives us the sum of squares error between the sample variogram and the fitted variogram model for $t = 1, \ldots, 4$ from both models under the given threshold of the grid. From this table we cannot draw a simple conclusion about which model is better, since different models generate smaller SSE on different days. Therefore we cannot simply choose one "better" model based on the SSE on one single day. If we are able to input more information, such as the altitude of locations (another factor affecting the water level), then Universal Kriging would be a good choice. In order to evaluate the both models, we calculate the sum of the SSE for $t = 1, \ldots, 365$, and the Universal Kriging model gives the smaller value of the sum of SSE 15.431 for our case.

Ultimately, we want to know: (1) if, after we narrow down and localize the Kriging space, the predictor will be more accurate or not; (2) how the Kriging predictor differs between subareas, based on the information from Helgoland.

To this end I divide the whole area into three subareas, all of which includes Helgoland: Area-up, Area-right and Area-down. In each area, the stations are located in a more narrow direction, so we might be able to avoid the anisotropy problem. Here I use the Ordinary Kriging for modeling, so that we can avoid creating a grid map for each subarea. However, from Figure 6.7 it is clear that the prediction error gets larger as the number of observations decreases, therefore we can conclude that Kriging in smaller spaces is not a suitable method for our case. Because of too few observations in each subarea, we can only obatain the fitted variogram with estimated parameters, but not the fitted variogram curve in the plot.

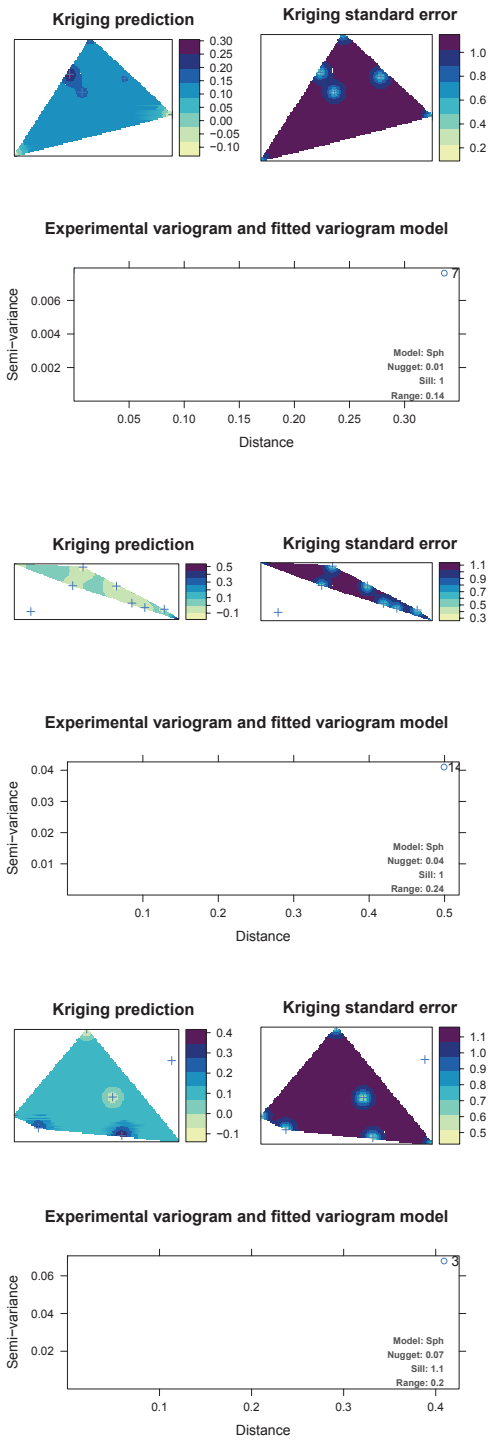

Figure 6.7.: The fitted variogram and Ordinary Kriging model in three subareas.

7. Conclusions and Further Work

We applied stochastic time series approaches to the water level data via different procedures and after the comparison of the empirical results, we chose the "best" model to capture conditional mean dynamics: detrending and deseasonalizing the data jointly, and then running an AR process. After that we fit the volatilities by a Fourier Series model and the conditional volatility dynamics were captured well. It turns out that this method functions well in general for our water level data, with unlike the temperature modeling, no cyclical part left in the volatilities.

In the second part of the paper, the residuals from the time series models were analyzed using spatial models. Both Ordinary Kriging and Universal Kriging based on the variogram model gave us similar predictors, but sometimes the Ordinary Kriging predictors were over smoothed. The visual results of Ordinary Kriging in subareas provide evidence that smaller sample sizes lead to less precise predictors.

In further work, we might consider simulating the values in other observed locations by using the residuals in Helgoland, based on the variogram, correlation, and geometric information. Then we can return to a time series model to predict water level in other locations, and use these observations to evaluate our model.

A. Appendix

	Bremen		Schulau		Cuxhaven		Hoernum	
	Estimate	p-value	Estimate	p-value	Estimate	p-value	Estimate	p-value
β_0	747.875	<2E-16	677.324	<2E-16	648.193	<2E-16	601.678	<2E-16
β_1	0.112	0.0743	0.139	0.0182	0.097	0.0702	0.072	0.1217
$a_{c,1}$	5.424	0.4918	6.315	0.3945	-6.319	0.3501	-12.375	0.0367
$a_{s,1}$	-1.015	0.7427	-0.660	0.8202	-0.503	0.8494	10.440	0.0009
$a_{c,2}$	-9.175	0.0548	-10.175	0.0236	-9.021	0.0277	-11.205	0.0018
$a_{s,2}$	-2.803	0.3646	-5.668	0.0516	-0.741	0.7795	0.396	0.8641
$a_{c,3}$	-2.796	0.4763	-3.425	0.3533	-2.163	0.5201	-5.857	0.0467
$a_{s,3}$	-2.296	0.4576	0.769	0.7913	-1.235	0.6410	-1.144	0.6209
$a_{c,4}$	4.228	0.2384	6.483	0.0548	4.976	0.1056	0.986	0.7132
$a_{s,4}$	-9.777	0.0017	-9.391	0.0013	-8.415	0.0016	-6.408	0.0059
$a_{c,5}$	10.355	0.0026	10.646	0.0010	7.215	0.0140	4.254	0.0965
$a_{s,5}$	-6.173	0.0464	-7.264	0.0128	-6.138	0.0209	-6.067	0.0090

Table A.1.: The coefficients of trend and Fourier Series from Model B and their corresponding p-values.

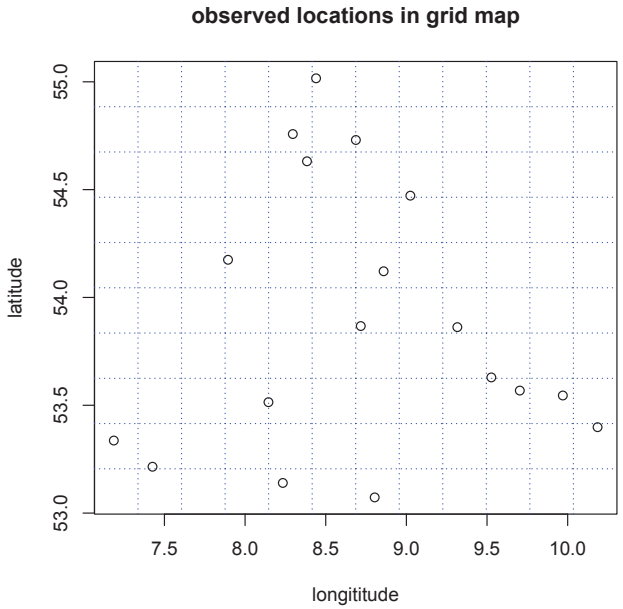

Figure A.1.: The grid map with the observed locations.

	Bremen		Schulau		Cuxhaven		Hoernum	
Lag L	Estimate	p-Value	Estimate	p-Value	Estimate	p-Value	Estimate	p-Value
1	0.458	<2.0E-16	0.488	<2.0E-16	0.472	<2.0E-16	0.506	<2.0E-16
2	0.068	<2.0E-16	0.011	0.17481	0.036	5.4E-06	-0.010	0.19389
3	-0.029	0.00040	-0.018	0.02347	-0.021	0.00886	0.006	0.41748
4	-0.039	7.9E-07	-0.036	7.3E-06	-0.045	1.8E-08	-0.038	1.8E-06
5	-0.051	9.4E-11	-0.048	1.0E-09	-0.053	2.0E-11	-0.048	2.6E-09
6	-0.061	8.3E-15	-0.049	6.5E-10	-0.060	4.1E-14	-0.042	2.0E-07
7	-0.048	8.2E-10	-0.047	3.4E-09	-0.052	3.5E-11	-0.044	5.4E-08
8	-0.060	2.5E-14	-0.054	8.3E-12	-0.062	4.1E-15	-0.055	9.2E-12
9	-0.036	3.9E-06	-0.029	0.00033	-0.036	5.5E-06	-0.028	0.00054
10	-0.035	1.0E-05	-0.030	0.00013	-0.032	5.7E-05	-0.028	0.00043
11	-0.026	0.00108	-0.025	0.00179	-0.026	0.00119	-0.026	0.00126
12	-0.036	4.0E-06	-0.051	1.5E-10	-0.048	9.9E-10	-0.055	9.1E-12
13	-0.021	0.00779	-0.027	0.00072	-0.025	0.00144	-0.034	2.4E-05
14	-0.005	0.55603	-0.016	0.04565	-0.009	0.28035	-0.016	0.04135
15	-0.008	0.30097	-0.020	0.01281	-0.014	0.08001	-0.018	0.02770
16	-0.023	0.00377	-0.031	8.6E-05	-0.030	0.00013	-0.043	6.2E-08
17	-0.045	9.2E-09	-0.038	2.2E-06	-0.038	1.8E-06	-0.033	4.5E-05
18	-0.036	3.8E-06	-0.035	1.2E-05	-0.037	3.9E-06	-0.036	5.5E-06
19	-0.053	1.8E-11	-0.047	3.1E-09	-0.055	4.5E-12	-0.047	4.4E-09
20	-0.044	1.7E-08	-0.034	1.8E-05	-0.040	5.7E-07	-0.028	0.00040
21	-0.040	4.9E-07	-0.039	7.1E-07	-0.045	1.5E-08	-0.042	1.3E-07
22	-0.047	2.8E-09	-0.038	1.5E-06	-0.043	5.0E-08	-0.024	0.00280
23	-0.021	0.00704	-0.015	0.05651	-0.022	0.00464	-0.016	0.05272
24	-0.042	1.1E-07	-0.040	5.1E-07	-0.036	4.1E-06	-0.029	0.00033
25	0.001	0.84969	-0.003	0.68360	-0.003	0.66209	-0.011	0.16733
26	-0.008	0.28335	-0.019	0.01626	-0.013	0.09874	-0.021	0.00881
27	-0.009	0.24948	-0.019	0.01680	-0.011	0.17734	-0.022	0.00596
28	0.021	0.00766	0.003	0.68171	0.011	0.18155	0.002	0.81040
29	0.003	0.67302	-0.021	0.00385	-0.001	0.84043	-0.030	2.2E-05

Table A.2.: The coefficients of AR process from Model B and their corresponding p-values.

	Bremen		Schulau		Cuxhaven		Hoernum	
Q	Estimate	p-Value	Estimate	p-Value	Estimate	p-Value	Estimate	p-Value
b_0	913.117	<2.0E-16	1097.58	<2.0E-16	867.558	<2.0E-16	704.09	<2.0E-16
$b_{c,1}$	-2.659	0.90316	-30.57	0.34845	-44.054	0.06877	-24.77	0.188430
$b_{s,1}$	666.673	<2.0E-16	827.71	<2.0E-16	706.962	<2.0E-16	585.39	<2.0E-16
$b_{c,2}$	16.023	0.46353	46.49	0.15428	9.667	0.68898	23.10	0.219932
$b_{s,2}$	25.819	0.23780	87.99	0.00722	74.202	0.00227	69.37	0.000259
$b_{c,3}$	3.207	0.88331	34.82	0.28566	11.865	0.62327	20.62	0.273450
$b_{s,3}$	-62.998	0.00415	-64.31	0.04906	-54.121	0.02554	-36.60	0.052290

Table A.3.: The coeffieciens of fitted volatility Model B. and their corresponding p-values.

t	Min.	1st Qu.	Median	Mean	3rd Qu.	Max.
1	-0.1503	-0.0743	0.0429	0.0889	0.1823	0.5752
2	-0.4337	-0.1826	0.0235	-0.0058	0.1183	0.3991
3	0.2205	0.3614	0.3972	0.4102	0.4565	0.6113
4	-0.5087	-0.3641	-0.1837	-0.2139	-0.0804	0.0435

Table A.4.: The summary statistics of the residuals $\hat{\varepsilon}_t$ when $t = 1, \ldots, 4$.

Bibliography

Anthoni, J. F. (2000). Oceanography. http://www.seafriends.org.nz/oceano/waves.htm.

Benth, F. E. and Saltyte Benth, J. (2005). Stochastic modelling of temperature variations with a view towards weather derivatives. *Applied Mathematical Finance*, 12(1):53–85.

Benth, F. E. and Saltyte Benth, J. (2011). A critical view on temperature modelling for application in weather derivatives markets. *Energy Economics*, doi: 10.1016/j.eneco.2011.09.012.

Campbell, S. D. and Diebold, F. X. (2002). Weather forecasting for weather derivatives. *Working paper*.

Campbell, S. D. and Diebold, F. X. (2005). Weather forecasting for weather derivatives. *Journal of the American Statistical Association*, 100(469).

Cressie, N. (1990). The origins of kriging. *Mathematical Geology*, 22:239–252.

Cressie, N., editor (1993). *Statistics for Spatial Data*. Wiley-Interscience.

Cressie, N. and Wikle, C. K., editors (2011). *Statistics for Spatio-Temporal Data*. Wiley.

Haberlandt, U. (2007). Geostatistical interpolation of hourly precipitation from rain gauges and radar for a large-scale extreme rainfall event. *Journal of Hydrology*, 332:144–157.

Härdle, W. K., López Cabrera, B., Okhrin, O., and Wang, W. (2011). Localising temperature risk. *FB 649 Discussion Paper*, 001.

Hengl, T., editor (2011). *A Practical Guide to Geostatistical Mapping*. University of Amsterdam Press.

Hengl, T., Heuvelink, G., and Stein, A. (2004). A generic framework for spatial prediction of soil variables based on regression-kriging. *Geoderma*, 120:75–93.

Koehler, A. B. and Murphree, E. S. (1988). A comparison of the akaike and schwarz criteria for selecting model order. *Journal of the Royal Statistical Society. Series C (Applied Statistics)*, 37(2):187–195.

Kumar, D. and Ahmed, S. (Jan. 2006). Seasonal behaviour of spatial variability of groundwater level in a granitic aquifer in monsoon climate. *Current Science*, 84(2).

Lamb, H. and Frydendahl, K., editors (1991). *Historic Storms of the North Sea, British Isles and Northwest Europe.* Cambridge University Press, Lawrence,Kansas, USA.

Olea, R. A., editor (1999). *Geostatistics for Engineers and Earth Scientists*. Kluwer Academic Publishers, Lawrence,Kansas, USA.

QSR (2000). Quality status report 2000 for the north-east atlantic. http://www.ospar.org/eng/doc/pdfs/qec2.pdf.

Stein, M. L., editor (1999). *Interpolation of Spatial Data*. Springer, Chicago, USA.

Stroud, J. R., Mueller, P., and Sanso, B. (2001). Dynamic models for spatiotemporal data. *Royal Statistical Society*, 63(673–689).

List of Figures

List of Tables

Declaration of Authorship

I hereby confirm that I have authored this master thesis independently and without use of others than the indicated sources. Where I have consulted the published work of others, in any form (e.g. ideas, equations, figures, text, tables),this is always explicitly attributed.

Berlin, February 15th, 2012 Xiaofeng Cao

Selbständigkeitserklärung

Ich erkläre, dass ich die vorliegende Arbeit selbständig und nur unter Verwendung der angegebenen Literatur und Hilfsmittel angefertigt habe.

Berlin, den 15.02.2012 Xiaofeng Cao